Chapter-2

Synthesis, Characterizations and Analysis Techniques

CHAPTER 2: Synthesis, Characterizations and Analysis Techniques

2.1 Overview

In order to accomplish the objectives discussed in chapter 1, it is essential to synthesize the investigated system and characterize them for their further analysis. This chapter describes the synthesis methods, characterization with distinct techniques, and the applied experimental techniques to evaluate the various properties of the proposed systems. In the present work, the proposed compositions (a) Sodium bismuth titanate ($Na_{0.5}Bi_{0.5}TiO_3$) (b) Non-stoichiometric $Na_{0.5+x}Bi_{0.5-x}TiO_3$; (x = -0.02, -0.01, 0.00, 0.01, 0.02) (c) Magnesium doped non-stoichiometric $Na_{0.5}Bi_{0.49}Ti_{1-x}Mg_xO_{3-\delta}$; (x = 0.00, 0.01, 0.02, 0.03) (d) Pure and alkaline earth metal substituted Tri-yttrium gallate $Y_{(3-0.06)}M_{0.06}GaO_{6-\delta}$; (M = Ca^{2+}, Sr^{2+} & Ba^{2+}) and (e) Co-doped tri-yttrium gallate $Y_{2.94}Ca_{0.06}Ga_xMg_{(1-x)}O_6$ (x=0.00, 0.01, 0.02, 0.03, 0.04) were prepared. The compositions listed in a, b, d, e have been prepared via solid-state reaction route and the compositions listed in c was prepared by polyol synthesis method. The physical properties such as structural, optical, thermal, and electrical have been analyzed for all synthesized materials with varying compositions. This chapter has been divided into three sections:

(1) Materials synthesis: The sample preparation and processing of materials with various compositions have been discussed in this section.

(2) Characterization techniques: This section briefly discusses the structural, microstructural, thermal, optical, and electrical characterization techniques used in the current investigation.

(3) Data analysis techniques: In this section, we have outlined analysis techniques, including Rietveld refinement of the X-ray diffraction (XRD) pattern, electrical conductivity, and impedance spectroscopy.

2.1.1 Specification of Raw Materials

High purity raw materials were used to synthesize the investigated compositions. The specifications of raw materials are listed in Table 2.1.

Table 2.1: Description of the raw materials with their chemical formula, purity, and manufacturer used for the preparation of proposed compositions

S. No	Raw Materials	Chemical Formula	Purity	Manufacturer
1.	Sodium Carbonate	Na_2CO_3	99.5%	Rankem
2.	Bismuth Oxide	Bi_2O_3	99%	SRL
3.	Titanium Oxide	TiO_2	99%	Merck
4.	Titanium Isopropoxide	$C_{12}H_{28}O_4Ti$	99.95	Alfa Aesar
5.	Yttrium Oxide	Y_2O_3	99.9%	Alfa Aesar
6.	Gallium Oxide	Ga2O3	99.99%	Alfa Aesar
7.	Calcium Carbonate	CaCO3	99.5%	Alfa Aesar
8.	Magnesium Oxide	MgO	98%	Merck

A few other high-grade chemicals, reagents, and solvents like ethanol, acetone, urea, ethylene glycol, isopropanol, nitric acid, deionized water, hydrochloric acid, etc. were also used to fabricate the samples.

2.2 Materials Synthesis

Sodium bismuth titanate ($Na_{0.5}Bi_{0.5}TiO_3$) and tri-yttrium gallate (Y_3GaO_6) can be synthesized by a number of ways, such as hydrothermal, molten salt, sol-gel, citrate method, topochemical microcrystal, etc. Each method has its own advantage and disadvantage. In the solid-state ceramic processes, high sintering temperature is required for densification, which is not economical and can allow volatile elements like Na and Bi to be lost due to their high volatile nature at high temperatures. Recently, the use of chemical routes has attracted researchers. The use of a precursor solution produces homogenous, reactive powders that densify the sample at lower temperatures while preventing the loss of volatile components. In the present work, we have synthesized the samples via solid-state reaction route and polyol mediated synthesis technique.

The details of preparative methods, experimental techniques and the basic working principle of the instruments used are summarized and presented subsequently in this chapter.

2.2.1 Solid-State Reaction Route (SSR)

The solid-state reaction route (SSR) is an extensively used technique for the synthesis of polycrystalline solids from constituent solid starting materials. It involves mechanical mixing of oxide powders, carbonates, followed by heat treatment. Generally, solids do not react at room temperature over an ordinary time scale. So, it is necessary to heat them at a much higher temperature. Factors that influence the solid-state reaction rate are structural properties of solids, reaction conditions, surface area, temperature, pressure, thermodynamic free energy change associated with the reaction[117][118]. The advantages associated with this method are given below:

1. Limited formation of side products
2. No solvents are needed in the reaction.
3. Structure purity along with desired properties.
4. Large scale production
5. Environment-friendly
6. Simplicity and low cost

A detailed procedure of the solid-state reaction route is shown in the schematic block diagram of Fig. 2.1.

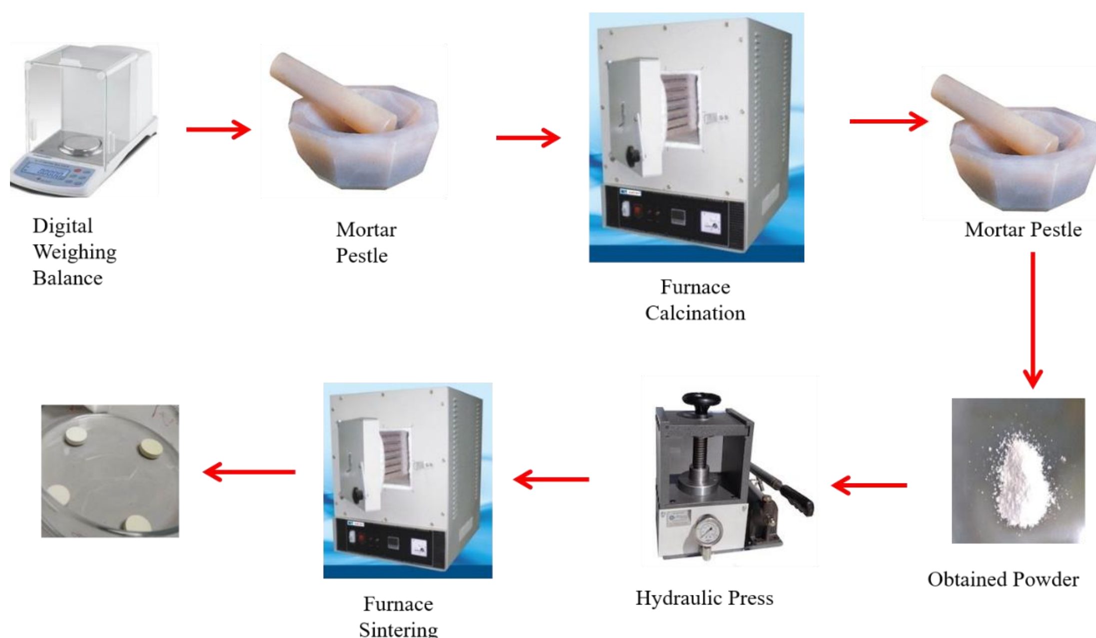

Figure 2.1: Schematic of Solid-state reaction route

2.2.2 Polyol-mediated synthesis route

Polyol process is a unique soft chemical method for the preparation of a variety of nanoparticles[119]. The cornerstone of this technology is the precipitation of solid materials in multivalent and high-boiling point alcohols such as ethylene glycol while heating with

adequate precursors (EG). The alcohol functions as a stabiliser, limiting particle development and preventing particle agglomeration. In this method, the appropriate amount of the constituent oxides were dissolved separately in concentrated nitric acid. Then these solutions were mixed in a conical flask and kept for magnetic stirring at 80-90 °C. After some time, double stage distilled water was added three to four times to eradicate the surplus acids. In this solution, 100 ml of EG was added into the five grams of urea (NH_2CoNH_2) dissolved double-distilled water. In order to achieve the uniform mixing of the solution, the solution was kept for constant stirring for about 2 hrs. After that, this mixed solution was heated around ∼100-120 °C to get the white precipitates. In this nano-powder synthesis approach, EG molecules behave as a solvent in addition to capping agent for reaction media. As the nucleation begins, neighbouring EG molecules cap smaller particles which moderate the particle growth rate. This also helps in hindering the agglomeration process of particles. The EG dielectric media of reaction also supports in controlling particle size. The obtained precipitate was eroded 2-3 times in ethanol in order to eliminate the extra EG and then kept for two days at room temperature to dry it. And after crushing, the as-prepared compositions were annealed at 500 °C in the air for 4h. EG (the capping agent) was eliminated in the burning process as carbon dioxide and water vapour phases. The flow chart of the synthesis process is represented in Fig. 2.2. Thus, the uncapped particles were obtained, and hence the growth of particles occurs. The advantages associated with this method are given below:

1. Produces fine and homogenous powder
2. Limited particle growth and prohibits the agglomeration of particles
3. Narrow particle distribution and high specific surface area
4. Controlled morphology

5. Low sintering temperature

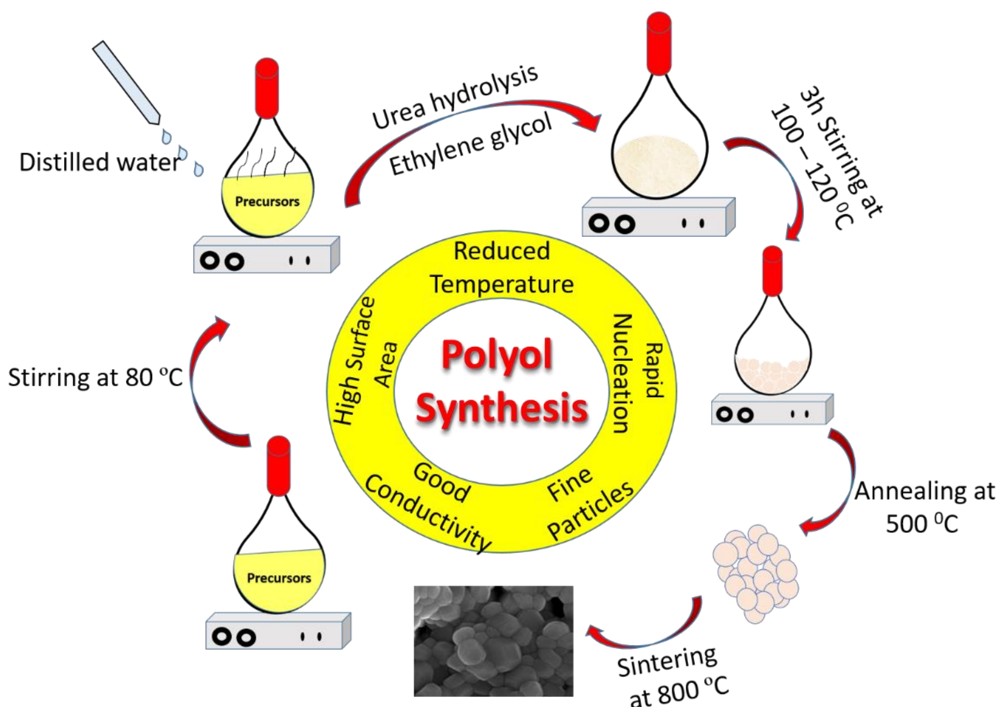

Figure 2.2: Schematics of polyol mediated synthesis process

2.3 Pelletization for Conductivity and Dilatometry Measurements

Pellets of the synthesized samples are formed using a hydraulic press machine (shown in Fig. 2.3). It involves mechanical or hydraulic pressure to pack the powder into a pellet in the die set. The pressure needed to form a pellet of adequate mechanical strength depends on the properties of the materials used, including but limited to particle size, adhesive material, and moisture level. Besides, binding agents like stearic acid, polyvinyl alcohol, and ethanol also assist pellet formation. Once the pellet is formed, pellets are placed into a furnace and heated at the desired temperature. This removes the binder residue, increases the density and mechanical strength of the material.

In this thesis, all the pellets were formed using a manual hydraulic press, die of 12 mm diameter and pressure of 6 tons.

Figure 2.3: Experimental setup of hydraulic press machine

2.4 Characterization Techniques

2.4.1 Thermal Analysis (TGA-DTA)

Differential Scanning calorimetry is a thermoanalytical technique that measures the heat flow into and out of the sample as a function of temperature or time while the sample is subjected to a controlled temperature program. In this method, powdered test materials are placed in a small capsule, generally alumina or other suitable refractory materials. Adjacent to the test sample, a second capsule containing an inert powder such as α-Al_2O_3, which does not exhibit endothermic or exothermic effects, is placed. The sample and the reference material are placed symmetrically in the furnace. The sample of known mass is heated or cooled, and during this process, the change in heat capacity is recorded in terms of heat flow. It is a very

potent technique to evaluate various material properties such as glass transition temperature, crystallization, thermal stability, melting, specific heat capacity, purity, and oxidation behaviour.

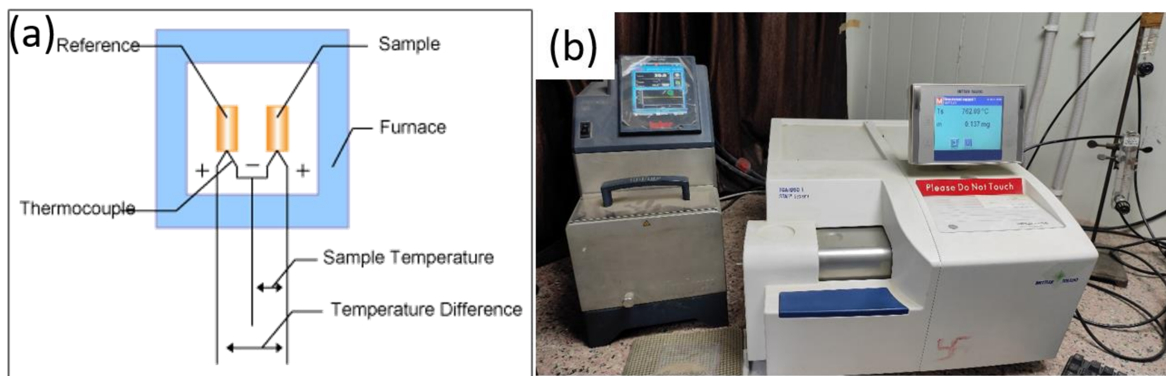

Figure 2.4: (a) The schematic representation and **(b)** experimental setup of TGA/DSC (right) [Central instrument facility (CIF) IIT (BHU)]

TGA is a method of determining the change in mass of a sample as a function of temperature or time in a controlled environment. It is used to determine the calcination temperature and thermal stability of the sample. If the mass of the sample remains constant in the given temperature range, then the sample is said to be thermally stable in that specific temperature range. Also, TGA provides information about the upper limit of temperature beyond which the sample starts degrading. The weight losses are fundamental properties of the sample and can be used for quantitative calculations of compositional changes etc. A phase transition in the sample may also be confirmed by using this technique.

In the present thesis work, TGA measurement was recorded using TGA/DSC 1 (Mettler Toledo, Germany) model in the nitrogen and oxygen atmosphere and operated within the temperature range from 27 ºC-1000 ºC. The schematic diagram and experimental setup of the TGA/DSC technique are shown in Fig. 2.4.

2.4.2 X-Ray Diffraction Analysis (XRD)

The powder X-ray diffraction technique (XRD) is a non-destructive and versatile analytical technique used to reveal detailed information about the crystallographic structure of the materials. XRD is based on elastic scattering, i.e. the change in the direction of em waves. The coherent sum of all the electromagnetic waves that are diffused from the atoms belonging to the same family of planes results in the diffraction pattern. All the materials provoke a distinct XRD pattern, which is indexed to identify various phases present in the material. Phase identification using XRD mainly depends on the peak position and relative intensities of these peaks in the diffraction profile. Most commonly, the X-ray radiations are emitted by the copper specimen, and its characteristic wavelength is 1.5418 Å for K_α radiation. Figure 2.5(a) and 2.5 (b) depicts the Braggs scattering from the lattice plane and block diagram of powder X-ray diffractometer.

2.4.3 Bragg's law

The X-ray diffraction (XRD) method follows Bragg's law of X-ray diffraction. This law can be explained geometrically, as depicted in Fig. 2.5. In XRD, a collimated beam of X-rays is incident on the crystallographic lattice plane with an interplanar spacing d_{hkl}. Let θ be the angle of incidence between the X-ray beam and lattice plane, the interplanar spacing d_{hkl} creates a path difference for the ray scattered from the top & bottom surface of the plane. Using the geometry, the path difference between incident and diffracted ray is found to be $2d_{hkl}\text{Sin}\theta$. If the path difference is an integral multiple of wavelength (λ), then the interference between the scattered rays can be said to be constructive. Mathematically, Bragg's law is given as:

$$2d_{hkl}\text{Sin}\theta = n\lambda \quad (2.1)$$

where n is an integer and is said to be an order of diffraction.

The geometry used in the X-day diffractometer is depicted in Fig. 2.5(b). The angle of incidence and scattered ray with respect to specimen surface is θ. The XRD pattern is recorded by deviating the incident X-ray beam angle by θ and scattering angle by 2θ. The scattered intensity is recorded as the function of 2θ. In some of the cases, the X-ray source is kept at a stationary position while the sample and detector are rotated by angle θ and 2θ, respectively. However, in most cases, the sample retains a stationary position while both the detector and source simultaneously rotate by θ angle. The central part of the diffractometer is Goniometer, and such precise rotation is performed by it. Generally, the sample has been mounted on a rotational axis, and the detector and X-ray source moves along its periphery. Normally, the 2θ range between 20° - 80° is sufficient to cover the most useful part of the diffraction pattern.

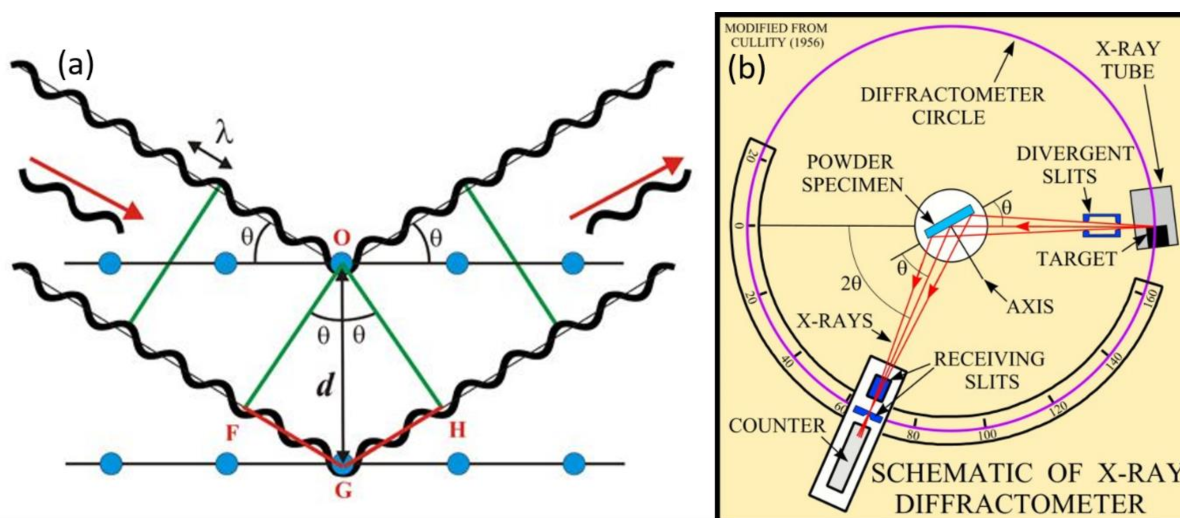

Figure 2.5: (a) Visualization of Bragg's law **(b)** Schematic representation of θ/2θ diffraction in Bragg-Brentano geometry

To check the phase formation of the studied compositions, XRD pattern was recorded using an X-ray diffractometer (Rigaku Miniflex II) applying Cu-Kα radiation with Ni filter and applied voltage of 40kV. The X-ray diffractometer used in our investigation is shown in

Fig. 2.6. The XRD peaks are generated from the randomly oriented planes identified by the respective Miller indices (hkl).

Figure 2.6: Experimental setup of X-ray diffractometer CIF IIT (BHU) [Rigaku Miniflex II, Japan]

The X-ray peaks are matched and indexed by the standard phase, which contains miller indices, diffraction angle or similar interplanar spacing, relative intensity and other crystallographic information. The "**International Center for Diffraction Data (ICDD)**," formerly known as the "**Joint Committee for Powder Diffraction Standards (JCPDS)**," maintains the standard database. Another alternative method besides this is the simulation technique in which the theoretical XRD pattern is generated by a computer program through structural information accessible from the ICDD database. This method is only applicable when the crystal phase or similar structure file is available in the ICDD database. The computed XRD pattern is then refined to fit the experimental XRD data by adjusting the instrumental, microstructural, and structural parameters via continuous iteration process.

In addition, the XRD pattern can also be used to calculate the crystallite size (d) of material[120]. Strain and the size of the crystalline domains both affect peak broadening. The Scherrer formula $\boldsymbol{d} = \frac{0.9\,\lambda}{\beta \cos\theta}$[121] can be used to calculate domain size, which was previously known as crystallite size. The programme FullProf suite was used to do the Rietveld refinement analysis of the XRD pattern, which is detailed in more detail later in this chapter.

2.4.4 Fourier Transform Infrared Spectroscopy (FTIR)

Infrared spectroscopy is an important tool for the vibrational study of the material. It detects molecular vibration by absorbing infrared light or by inelastic scattering of the light by a molecule. The method is called FTIR spectroscopy because Fourier transform is carried out by the computer to convert raw data to actual spectrum. The spectrum is obtained in a short period of time. It is used to determine the functional group attached to an atom or molecule. A schematic diagram of the Fourier transform infrared spectroscope is shown in Fig. 2.7.

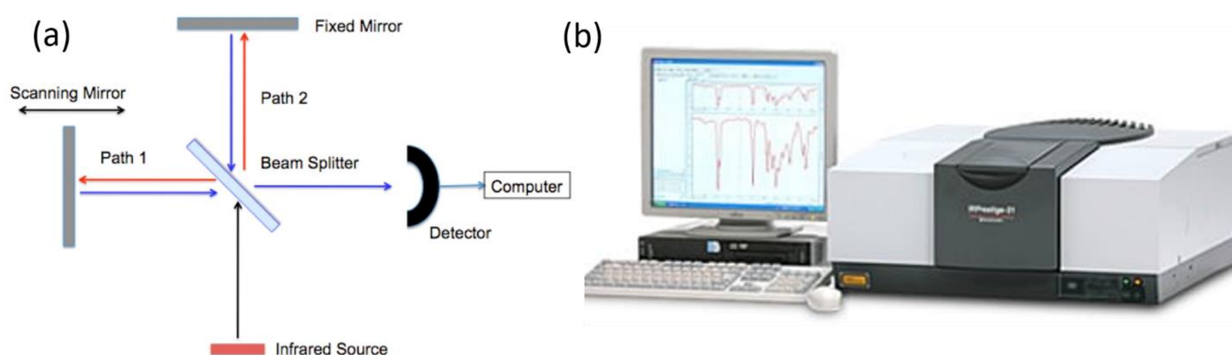

Figure 2.7: (a) Mechanism and **(b)** experimental setup of Fourier transform infrared spectroscopy

The most important part of the FTIR setup is the interferometer. A Michelson interferometer is usually employed in the FTIR spectrometer. It consists of two mirrors and a beam splitter (semitransparent mirror) placed at an angle of 45° to the fixed and moving mirror.

The beam splitter divides the beam and recombines with the fixed and moving mirror so that the recombined beam generates a wavelength-dependent interference pattern.

The beam splitter transmits half of the incident infrared beam and reflects the second half. The two splitted beams strike the movable and fixed mirror, respectively. After reflecting from both the mirrors, the splitted beam again combines at the beam splitter in order to irradiate the sample before being received by the detector. The interferogram is a cosine Fourier transform of the spectrum, and with the help of data station, the obtained data is Fourier transformed to the recognizable form. Most of the molecular vibration lies in the range of 400-4000 cm^{-1}.

In this thesis work, FTIR spectra of samples were recorded using FT-IR spectrophotometer of Shimadzu, model DF 803 Japan, in transmission mode with the wavenumber range of 400-4000 cm^{-1}. Samples under test were mixed with KBr, pelletized and used for measurement at room temperature.

2.4.5 Dilatometry

Dilatometry is the measurement of the expansion of material in response to the change in temperature. Most of the materials expand when heated, and by employing a dilatometer, this expansion can be measured. Most common dilatometry has a highly sensitive pushrod enclosed within a furnace. As the temperature of the furnace increases, the change in sample length is measured, and the thermal expansion coefficient can be calculated.

The physical, thermal expansion coefficient (α) can be calculated from slope of this elongation vs temperature curve by the following equation

$$\alpha_L = \frac{\Delta L}{L\Delta T} \tag{2.2}$$

where α is the thermal expansion coefficient, ΔT is the change in temperature, L is the initial length of the sample, and ΔL is the change in length. Dilatometry can also be configured to allow sample heating in different atmospheres, such as argon or hydrogen.

Thermal expansion occurs due to the increase in average bond length between atoms with the increase in temperature. When a material is heated, molecules start to vibrate and move, causing an increase in the interatomic distance. For materials having different structures, the overall expansion coefficient can be expressed as all the components of the structure. This is why TECs of the material must be checked to confirm material compatibility.

The thermal expansion coefficient (TEC) is an important characteristic for the application of SOFCs. Ideally, the TEC value of all the components should be similar at any temperature the cell may encounter. If the TEC values of cell components are widely different then, cracks or delamination may occur, which may cause the cell to cease working and become hazardous, especially if anode and cathode gases get mixed.

Figure 2.8: Experimental setup of Dilatometry for TEC measurement [NETZSCH DIL, 402 PC/4]

Within this thesis, dilatometry measurements were carried in the air out using Netzsch DIL 420 PC/4 dilatometer in the temperature range of 50-1000 °C and constant cooling and heating rate of 2 °C/min. The experimental setup for dilatometry is shown in Fig. 2.8.

2.4.6 BET Surface Area Measurements

BET theory was established by Stephen Brunauer, Paul Hugh Emmett, and Edward Teller in 1938. It was an extension of Langmuir's theory, which describes monolayer molecular adsorption to multilayer adsorption. It aims to explain the physical adsorption of the gas molecule on the solid surface and serves as an important tool for the estimation of the specific area of materials. This theory is based on the following hypothesis:

(a) Adsorption on a solid surface is uniform and localized, and adsorption at one site does not affect adsorption at other locations.

(b) Molecules can be adsorbed in the second, third...., and nth layers, with the nth layer's surface area equal to the $(n\text{-}1)^{th}$ layer's coverage.

(c) The adsorption energy in the first layer, E1, is considered to be constant, and the adsorption energy in subsequent layers is assumed to be the same as EL, the liquefaction energy of the gas.

On the basis of aforesaid assumptions, Brunauer, Emmett, and Teller derived the following equations, written as:

$$\frac{1}{\upsilon[(p_0/p)-1]} = \frac{c-1}{\upsilon_m}\left(\frac{p}{p_0}\right) + \frac{1}{\upsilon_m c} \quad (2.3)$$

$$c = \exp\left(\frac{E_1 - E_L}{RT}\right) \quad (2.4)$$

$$V_{liq} = \frac{P_a + V_{ads} + V_m}{RT} \quad (2.5)$$

where υ is the volume of adsorbed gas, υ_m is the volume of adsorbed as monolayer, p_0/p is the relative pressure, c is BET constant, E_1 is the heat of adsorption of the first layer, and E_L is adsorption heat for the second and higher layers, V_{liq} is the volume of N_2 in the pore, V_{ads} is the volume of gas adsorbed, V_m is the molar volume of liquid adsorbed, P_a is ambient pressure and T is temperature [122]. The plot of $P/\upsilon(P_o-P)$ against P/P_o should provide a straight line because c is a constant for a given gas and is a constant for a given gas-solid system. The slope of the linear plot yields $(c-1)/(\nu_m)$, while the intercept yields $1/(\nu_m)$. Both ν_m and c can be calculated based on the slope and intercept. At different temperatures, a wide number of gas adsorption isotherms on various adsorbents are determined. Figure 2.9 depicts the experimental setup for the BET analyzer.

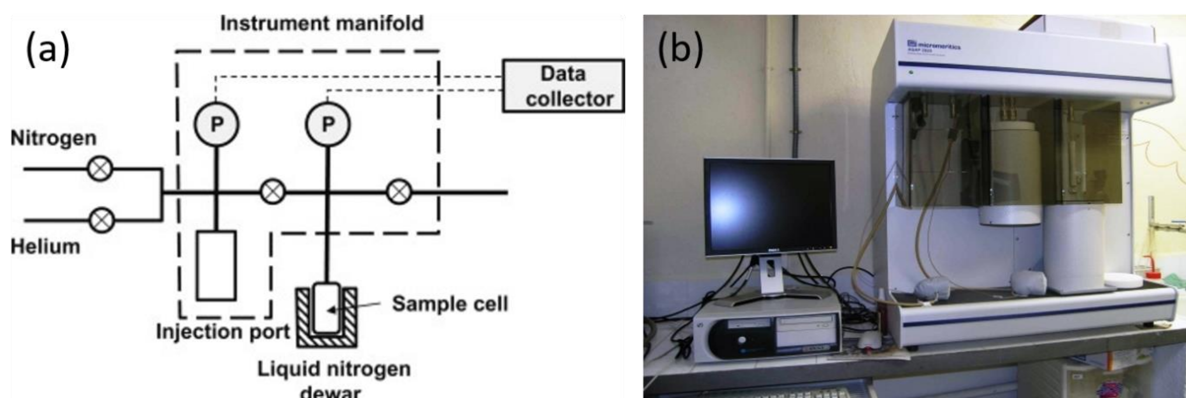

Figure 2.9:(a) Mechanism and **(b)** Experimental setup of porosity and BET surface area analyzer [Micromeritics ASAP 2020]

2.4.7 Raman Spectroscopy

Raman spectroscopy is an analytical technique that uses scattered light to measure a sample's vibrational energy modes. It's based on the interaction of light with a material's chemical bond. When light collides with the matter, the vast majority of photons scatter or

disperse with the same energy as the incident photon. Elastic scattering, often known as Rayleigh scattering, is a type of scattering. Only around one in every ten million photons will scatter at a different frequency than the incident photon. Inelastic scattering, often known as the Raman effect, is the name given to this mechanism. Raman spectroscopy can give both structural and chemical information, along with the identification of the substance through their characteristic Raman' fingerprint'.

When a photon is scattered by a molecule in Raman spectroscopy, the photon's oscillating electric field induces polarisation in the molecular electron cloud, leaving the molecule in a higher energy state. The photon's energy is transmitted to the molecule. The virtual state of the molecule can be thought of as the formation of a short-lived complex between the photon and the molecule. Because the virtual state is unstable, the photon is emitted right away.

The Raman spectrometer's working mechanism is depicted in Fig. 2.10. It is made up of four major components: (i) The source of excitation (LASER), (ii) Sample illumination, (iii) Light collecting optics, wavelength selector (Filter, spectrophotometer) (iv) Detector (Photodiode array, Charge-coupled devices, or Photo-multiplier-tube (PMT)). Depending on the availability of a spectrometer, the sample is usually illuminated by a laser beam in the ultraviolet (UV), visible (Vis), or near-infrared (NIR) spectrum. The dispersed light passes through the interference filter, is collected by the lens, and the Raman spectrum of the analyzed materials is recorded. Raman spectrum is an invaluable analytical tool, which gives information about molecular fingerprints as well as monitors changes in molecular band structure (e.g., state changes and stress & strain). The light coming from the excitation laser source interacts with the molecular vibrations, phonons or other excitations present in the

system under investigation. As a result energy of the laser photons is being shifted in either up or down direction, depicted in Fig. 2.10. Stokes Raman scattering occurs when a molecule absorbs energy from a photon during the scattering process. The dispersed photon loses some energy, and its wavelength rises. If the molecule loses energy by relaxing to a lower vibrational state, the scattered photon receives energy and its wavelength decreases. Anti-Stokes Raman scattering is the name given to this mechanism. Both Stokes and Anti-Stokes processes, according to quantum physics, are equally plausible. The majority of molecules in a group of molecules, on the other hand, are in the ground vibrational level. As a result, Stokes scatter is statistically preferable. As a result, when compared to the anti-Stokes scattering, Stokes scatter is more intense.

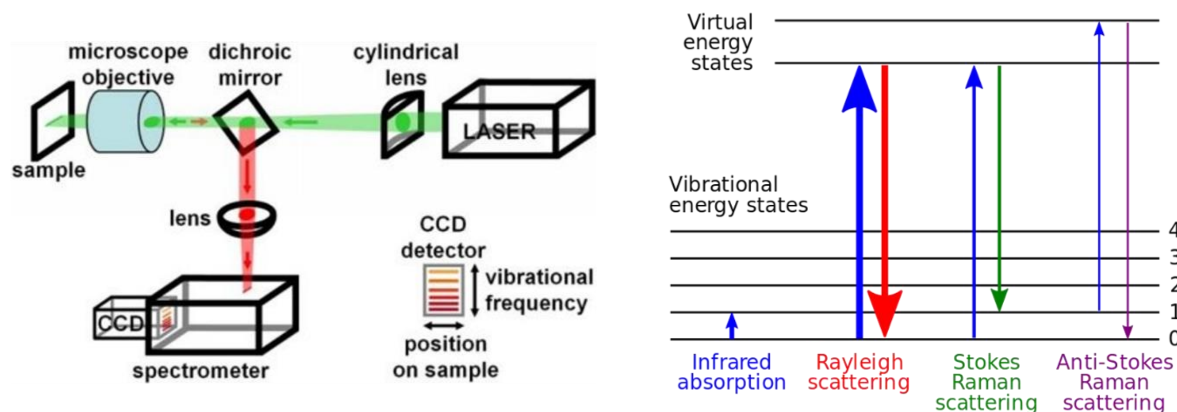

Figure 2.10: Schematic representation of the principle of Raman spectroscopy

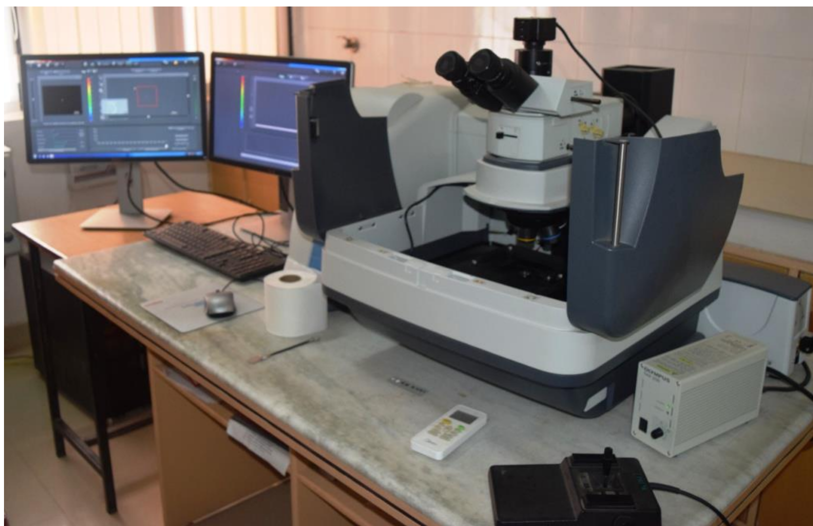

Figure 2.11: Experimental setup of DXRxi Raman measurement. (Banasthali University, Rajasthan)

In this thesis work, the Raman spectra of the investigated samples were recorded using DXRxi Raman imaging microscope by Thermo SCIENTIFIC with the excitation wavelength of 532 nm in the wavenumber range of 50 – 800 cm^{-1}, and the experimental setup is presented in Fig. 2.11.

2.4.8 X-Ray Photoelectron Spectroscopy (XPS)

XPS is the non-destructive surface-sensitive spectroscopic technique that measures the elemental composition at the part per thousand range, chemical and electronic state of the elements that exist inside the material, empirical formulae. It not only shows what elements are present but also the elements they are bound to. XPS is a high vacuum technique and operates at vacuum ~ 10^{-6} Pa. The current area of advancement is an ambient pressure XPS which can analyze the samples at numerous pressure of a few tens of millibars. This technique is based on the process of photoemission. In this technique, the material surface is bombarded with the high energy X-ray; as a consequence, the inner level electrons of the surface atom,

within 1-10 nm, absorb the photon energy hυ, overcome their binding energy E_B, and emitted out of the surface with the kinetic energy E_{kin} (depicted in Fig. 2.12). This process is described by the following Einstein equation:

$$E_{kin} = h\upsilon - E_B - W_f \tag{2.6}$$

where $h\upsilon$ is the energy of the incident X-ray source, E_{kin} is the kinetic energy of emitted electrons, W_f is the work function of the material, and E_B is the binding energy of core electrons. MgKα and AlKα are the two source sources generally used because of their high energy and narrow width.

The energy spectrum of the emitted photoelectrons are analyzed, and this gives a spectrum of intensity as a function of binding energy. The binding energy of each peak are characteristic of the element. XPS is also known as ESCA (Electron Spectroscopy for Chemical Analysis). Laboratory XPS easily detects all the elements except hydrogen and helium. XPS is routinely used to investigate semiconductors, metal alloys, inorganic compounds, catalysts, glues, polymers, ceramics, glasses, inks, woods, bones, teeth, medical implants, elements, bio-materials, viscous oils, ion-modified materials and many others.

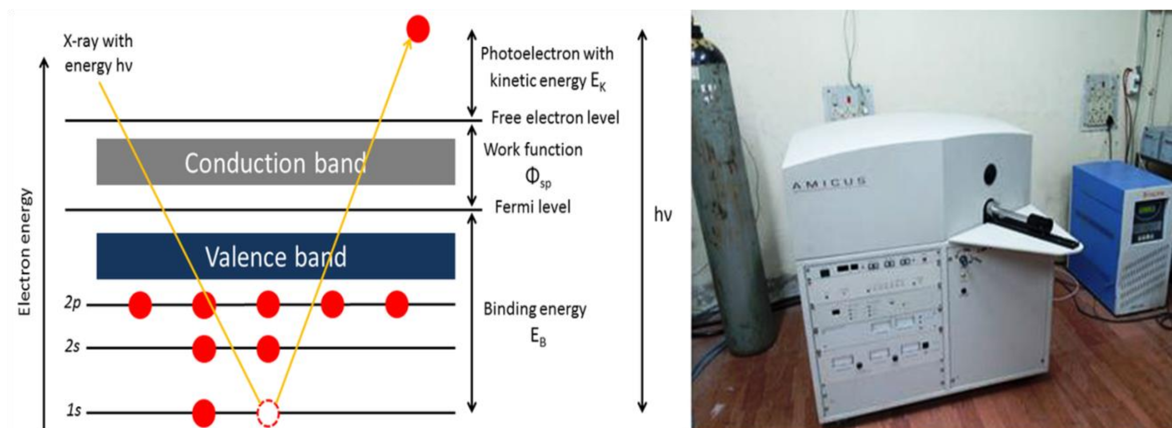

Figure 2.12: **(a)** Mechanism and **(b)** Experimental setup for the XPS spectroscopy (Kratos Amicus)

In the present thesis work, XPS spectra of the samples have been recorded using Kratos Amicus XPS setup utilizing Mg target under 10^{-6} Pa pressure.

2.4.9 Scanning Electron Microscopy (SEM)

Scanning electron microscope is a type of electron microscope that uses a highly focused electron beam to produce the image of the sample. When a high-energy electron beam collides with a sample's surface, it causes a variety of interactions that reveal details about the sample's chemical composition and morphology. Figure 2.13(a) illustrates the different electron-sample interactions.

For the electron beam to pass through the sample, the sample should be conductive. So in the case of nonconducting samples, a layer of gold is deposited on the surface of the sample.

In SEM, an electron beam of energy 5 to 30 keV emitted from the filament is accelerated towards the sample and focused by several condenser lenses. When this beam hits the surface of the sample, numerous collision between the electrons in the beam and atoms in the sample occurs. As a result of the collision, a few of the outermost electrons will be detached from the sample. These electrons, known as secondary electrons, have relatively lower kinetic energy and can be readily detected by the detector. The detector counts the number of emitted electrons, and the results are displayed on the computer screen. An enlarged image of the sample is generated by scanning the electron beam over a small area and detecting the number of electron beams arising from each point. Both the topology and atom number of the sample affect the number of secondary electrons emitted.

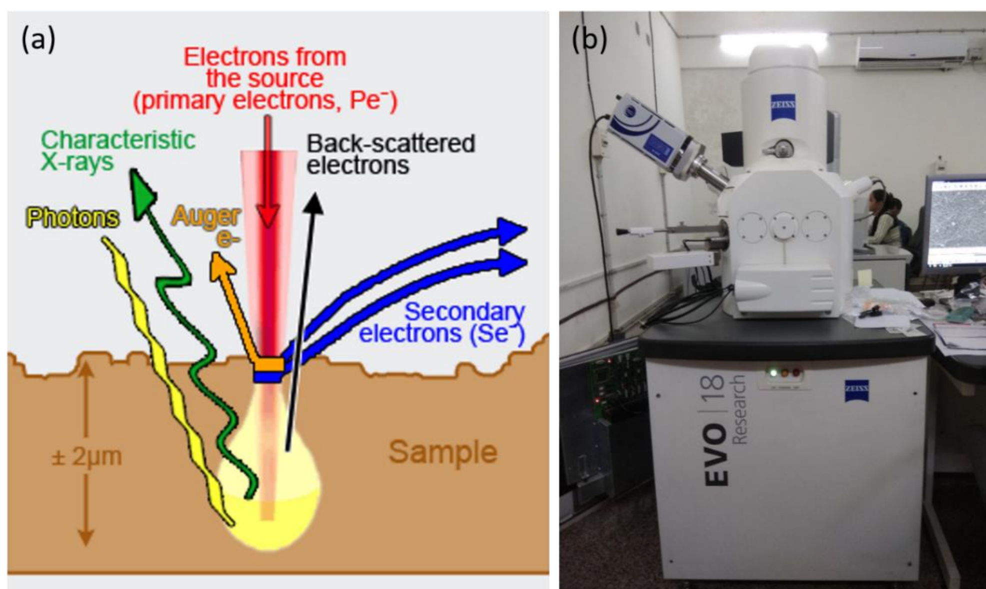

Figure 2.13: (a) Mechanism and **(b)** Experimental setup of SEM measurement (CIF-IIT (BHU))

To analyze the elemental composition, a facility attached with the SEM microscopy, generally known as energy dispersive X-ray analysis (EDAX or EDX). It uses X-ray analysis to look into the elemental composition and abundance. The target sample is attacked with high-energy electrons in this experiment. The incident electrons interact with the electron shell bound to the nucleus and eject them from the shell. This ejection of the electron leaves a void in the inner layer, and to fill it, an electron will jump from the higher energy shell to the lower energy shell, expelling energy equal to the difference in energy between the two energy levels. This energy radiate in the form of X-rays and are known as characteristic X-ray. Each element has a unique set of energy levels because of which energy of the X-ray produced will be different for different elements.

In the present thesis, EVO-MA15/18scanning electron microscope has been used in which EDS apparatus was attached for the compositional analysis, represented in Fig. 2.13(b).

2.4.10 Ultra-Violet Visible (UV-Vis) Spectroscopy

UV-Vis is a technique that involves absorption and/or reflectance of light (radiation) in the ultraviolet-visible spectral region. UV-Vis absorption spectroscopy measures the attenuation of the light beam after it passes through the sample or after reflection from the surface. The spectrometer measures the light intensity passing through the sample (I) and compares it with the light intensity before passing through the sample (I_o). The ratio of (I/I_0) is defined as transmittance, usually indicated in percentage form (%T). The relation between absorbance (A) and transmittance (T) is defined by the following equation:

$$A = -\log\left(\frac{\%T}{100\%}\right) \tag{2.7}$$

The four main components of the spectrometer are (a) light source, (b) sample holder, (c) diffraction grating in a monochromator or prism (d) detector. The radiation source is usually a Tungsten filament, deuterium arc lamp, Xenon arc lamp, or, more recently, light-emitting diodes. A photomultiplier tube, photodiode, charge coupled device (CCD) or a photodiode array is used as a detector. The photomultiplier tube and single photodiode detectors are used with scanning monochromator to filter out all wavelengths and pass only a single wavelength to the detector at one time. The diffraction grating is moved by scanning monochromator by "Step-through" every wavelength so that its intensity can be measured as a function of wavelength.

The optical bandgap of the investigated samples has been determined by using the UV-Vis data. The absorption data of UV-Vis spectrometer was used to determine the band gap (E_g) of the material. The band gap is calculated using the Tauc relation. According to the Tauc relation, the optical absorption strength depends on the difference between the photon energy and the band gap as follows:

$$\alpha h\upsilon = A(h\upsilon - E_g)^n \quad (2.8)$$

where h is Plank's constant, α is absorption coefficient, υ is photon's energy, A is proportionality constant, and E_g is band gap. The value of exponent n represents the nature of transition, whether allowed or forbidden and direct or indirect. n = ½ corresponds to direct allowed transition, n = 3/2 corresponds to direct forbidden transition, n = 2 for indirect allowed transition and n = 3 for indirect forbidden transition. The material studied in this thesis has an indirect allowed transition, n = 2.

Figure 2.14: Experimental setup of UV-Visible measurement[JASCO V-770 UV–Vis spectrometer]

In this thesis, UV-Visible absorption spectra were recorded using JASCO V-770 UV–Vis spectrometer in the wavelength range of 200-1000 nm.

2.4.11 Photoluminescence Spectroscopy (PL)

Photoluminescence spectroscopy (PL) is a non-destructive, contactless technique for probing a material's electrical structure. It is one of the many forms of luminescence and is initiated by photoexcitation; hence the prefix photo is used. In this process, a material absorbs

photon (electromagnetic radiation) and then re-radiates photon. In other words, this process describes an excitation to a higher energy state and then return to the allowed energy state accompanied by the emission of a photon. The time between absorption and emission is minimal. The quantum mechanics postulates are used to regulate the selection rules between states.

Photoluminescence is an essential method for measuring the purity and crystalline quality of semiconductors. Photoluminescence can be categorized as either intrinsic or extrinsic luminescence. Intrinsic luminescence occurs when light is emitted by a pure substance or crystal. This intrinsic luminescence is grouped in three categories: Band to band luminescence, cross luminescence, and exciton luminescence. Extrinsic luminescence occurs when impurities or defects are intentionally introduced into a phosphor. Figure 2.15 shows the schematic diagram of a photoluminescence spectrophotometer. This spectrophotometer exhibit a xenon lamp which is used as an excitation source. This lamp consists of high intensities of all wavelengths. Photoluminescence spectrophotometer is equipped with a monochromator to select a single wavelength used in both processes. The monochromator used in excitation contains two gratings, which decreases stray light, i.e., light with different wavelengths from the chosen one. In addition, to reduce stray light, the monochromator employs concave gratings created through holographic means. Both monochromators are motorized so that wavelength scanning can be done automatically. Photomultiplier tubes are used to detect the fluorescence, which is then multiplied by electronic devices. Typically, the output is presented in a graphical format and saved in a digital format.

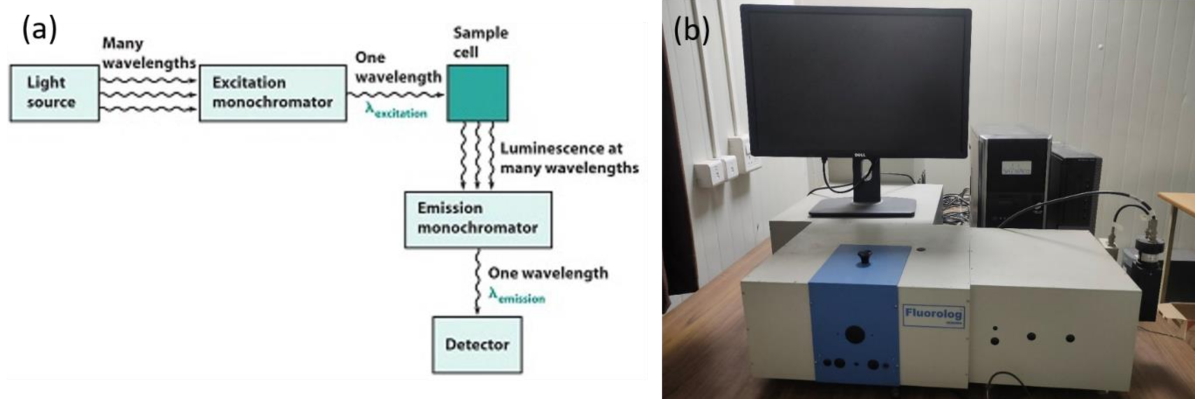

Figure 2.15: **(a)** Mechanism and**(b)** Experimental setup of photoluminescence spectroscopy [Horiba Flourolog 3]

In this thesis, Photoluminescence measurements were done using Photo-luminescence spectrometer Horiba Flourolog 3 (Japan) using Xe (xenon) lamp as an excitation source and slit width of 1nm.

2.4.12 Density Measurement

The density of the sintered samples were evaluated using the Archimedes principle. The powder samples were pelletized with the help of a hydraulic pressing machine by using a circular die. In this process, initially, the pellets are weighed in the air; thereafter, they are immersed in water as a liquid medium. The image of the density measurement kit (Sartorius, BSA2245-CW) is shown in Fig. 2.16. Archimedes's principle is represented by

$$D = \frac{w_1}{w_2} \times \rho, \tag{2.9}$$

where D is the density of the object, w_1 and w_2 are the weight of the sample and the weight of the water displaced, respectively, and ρ is the density of water. Theoretical density was obtained from the molecular weight of given compound and lattice parameters by using the above relation

$$D_{th} = \frac{n \times M}{N \times V} \tag{2.10}$$

where D_{th}, n, M, N, V represents the theoretical density, number of formulas per unit cell, molecular weight of the given compound, Avogadro's Number, and unit cell volume, respectively.

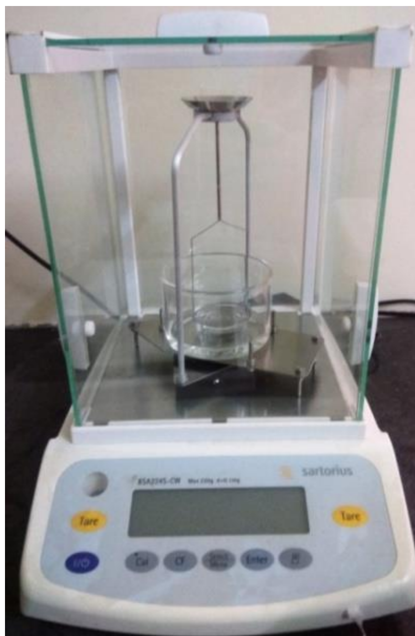

Figure 2.16: Density measurement kit by Sartorius, BSA2245-CW

2.5 Electrical Data Analysis

Electrochemical impedance spectroscopy is a powerful non-destructive technique to analyze the electrical properties of a material. It is useful to inspect the defects, microstructure, electrical conductivity, and surface chemistry of materials, including dielectrics, ionic conductors, and adsorbate-adsorbent interface[123]. On applying an alternating voltage or current to the sample, the conductivity, impedance, dielectric, and modulus properties are obtained[124][123].

For the electrical properties evaluation, the electrodes were created on both sides of pellets using high-temperature platinum paste. The platinum-coated pellets were then cured at

700 ºC for 30 minutes. The electrical response of different samples were then carried out in the ambient atmosphere by mounting the pellet in the sample holder inside a furnace using a two-probe LCR setup. The experimental setup used for the characterization is depicted in Figure 2.17. The temperature and frequency-dependent electrical response, such as dielectric constant, impedance, dielectric loss, complex modulus, etc., were measured with the help of Wayne Kerr 6500P series LCR meter in the temperature range of RT to 700 ºC and frequency range of 24 Hz to1 MHz.

Figure 2.17: Experimental set up of automated impedance analyzer along with sample holder and furnace (6500 P Wayne Kerr, UK)

With the help of these studies, ion relaxation and dynamics phenomenon can be understood. Initially, any two parameters such as conductance (G) and dissipation factor (D) can be calculated, and using these parameters; remaining parameters can be derived;

$$\text{Capacitance (C)} = \frac{G}{\omega D} \qquad (2.11)$$

$$\text{Conductivity } (\sigma) = G^*\left(\frac{d}{A}\right) \qquad (2.12)$$

$$\text{Dielectric constant } (\varepsilon_r) = \frac{C*d}{\varepsilon_0 * A} \tag{2.13}$$

$$\text{Real part of impedance } (Z') = \frac{D^2}{G*(1+D^2)} \tag{2.14}$$

$$\text{Imaginary part of impedance } (Z'') = \frac{Z'}{D} \tag{2.15}$$

$$\text{Real part of modulus } (M') = \omega * C_0 * Z'' \tag{2.16}$$

$$\text{Imaginary part of modulus } (M'') = \omega * C_0 * Z' \tag{2.17}$$

where A, d, C_0 are the cross-sectional area, thickness of the pellet and capacitance of free space, respectively. The capacitance of free space is given by C = $\frac{A\varepsilon_0}{d}$. After calculating the aforesaid parameters, the detailed study of different spectroscopic analysis has been carried out depending on the characteristics of the materials.

2.5.1 Impedance Spectroscopy Analysis

Dielectric and electrical properties of polycrystalline materials have contributions from (i) bulk or grains, (ii) grain boundaries, and (iii) electrode specimen interface or electrode polarization. So as to understand electrical behaviour and alter its properties, it is essential to separate these contributions. Impedance analysis is a powerful tool to separate the distinct contributions present in the electrical/dielectric properties of ceramics[124]. The AC response of any material can be expressed by four immittance functions. These are complex impedance (Z*), electric modulus (M*), admittance (Y*), and permittivity (ε*). These are related to each other as:

$$Z^* = Z' - iZ'' = \frac{1}{i\omega C_0 \varepsilon^*} \tag{2.18}$$

$$Y^* = Y' + iY'' = i\omega C_0 \varepsilon^* \tag{2.19}$$

$$M^* = M' + iM'' = \frac{1}{\varepsilon^*} \tag{2.20}$$

$$\varepsilon^* = \varepsilon' + i\varepsilon'' \tag{2.21}$$

For impedance analysis, two types of plots are generally used. (1) Complex plane plot, like, Z″ vs Z′ and M″ vs M′ plots and (2) Spectroscopic plots like, $\frac{Z''}{Z'}$ or $\frac{M''}{M'}$ vs logυ plots.

If a polycrystalline sample has all the three contributions, such as grain, grain boundary, and electrode, then each contribution can be presented by an equivalent circuit containing R and C connected in parallel. So the sample can be represented by an equivalent circuit containing three parallel RC circuits connected in series, as shown in Fig. 2.18. Nyquist plot (Cole-Cole) is majorly applied to calculate the frequency response information of any system by complex impedance function: $Z^*(\omega) = Z'(\omega) - iZ''(\omega)$, where $Z'(\omega)$ and $Z''(\omega)$ are the real and imaginary part of $Z^*(\omega)$. The real and imaginary part of total impedance of equivalent is given by:

$$Z' = \frac{R_g}{(1+\omega R_g C_g)^2} + \frac{R_{gb}}{(1+\omega R_{gb} C_{gb})^2} \tag{2.22}$$

$$Z'' = R_g \frac{\omega R_g C_{gb}}{(1+\omega R_g C_g)^2} + R_{gb} \frac{\omega R_{gb} C_{gb}}{(1+\omega R_{gb} C_{gb})^2} \tag{2.23}$$

where, R_g and C_g are the bulk (grain) resistance and capacitance, respectively, and R_{gb} and C_{gb} are the corresponding quantities for interfacial boundary (grain boundary). The relative position of the two arcs in the complex plane can be identified by frequency. In the complex plane, the arc of bulk lies in the higher frequency range than that of the grain boundary as the relaxation time for the grain boundary is higher than that of the bulk. R_g, R_{gb}, and R_{el} represents the relative contribution from grain, grain boundary, and electrode polarization

while C_g, C_{gb}, and C_{el} represents the corresponding capacitive contributions, respectively. In complex plane impedance and modulus analysis, one can observe three semicircular arcs if each of the contributions has a single value of relaxation time, as depicted in Fig. 2.18. Relaxation time (τ), which is equal to the inverse of angular frequency (ω) at which the relaxation peaks occur, is given by the RC product i.e.

$$\tau = 1/\omega = RC \tag{2.24}$$

Real axis intercept equations for various Immittance functions plane plots are given by Hirose and West[125].The intercepts of the arcs with the real axis (M') give the resistive contributions R_g, R_{gb}, and R_{el} in the impedance plots. The intercepts with M' axis in modulus plots is inversely proportional to the capacitive contributions (C_o/C_g, C_o/C_{gb} and C_o/C_{el}). The value of capacitance from the impedance plot and resistance from the modulus plot can be derived from the peak point frequency in the arc where ωRC = 1 is satisfied. Frequency increase in complex plane impedance and modulus plot are inverse to each other. In the complex impedance plot, electrode polarization appears in the lowest frequency range, followed by grain boundaries in the intermediate frequency range, and gain or bulk contribution appears in the highest frequency range. If the centre of the above three semicircle lies on the real axis, i.e., Z' and M', then it means that all the contribution has a single value of relaxation time. Contrary to this, if the centre of the semicircle lies below the real axis, then it means the distribution of relaxation times. The angle α, defined as the angle which the line joining the origin to the centre of the circle makes with the real axis, is a measure of the distribution of relaxation times of that contribution. The definite numbers of arcs appearing in the complex plane plot also depend on numerous time constants. An electronic specimen having the negligible value of electrode-specimen interface contribution (ohmic contact) can

be represented by two parallel RC elements connected in series. Bulk and grain-boundary conductivities σ_g and σ_{gb}, can be calculated respectively using relations $\sigma_g = (1/R_g)(t/A)$ and $\sigma_{gb} = (R_g C_b / R_{gb} C_{gb}).\sigma_g$ with C being the respective capacitances. The value of capacitance and resistance (i.e. C_g, C_{gb}, R_g, and R_{gb}) can be calculated from the best fit of the Cole-Cole plots at various temperatures. Full, partial, or no semicircle observed in the Cole-Cole plot, depends on the strength of relaxation, experimentally available frequencies and value of distribution parameters. Strength of relaxation is defined as $\varepsilon_S / \varepsilon_\infty$ where ε_S is the static dielectric constant value as $\omega \rightarrow 0$ and ε_∞ is the dielectric constant as $\omega \rightarrow \infty$ i.e. at optical frequencies. Therefore it is not astonishing that certain function is favoured on other depending on whether the material being explored is conducting, semiconducting or insulating[124]. From the above discussion, it is clear that impedance plots highlight circuit element (contribution) with large resistance (grain boundaries and electrode-specimen interface) while the modulus plots highlight the contribution with minimum capacitance (bulk contribution). Usually, we see three arc responses related to the bulk, grain boundary, and electrode relaxation. If the frequency range is not the limit, we may see all the processes related to the electrochemical reaction by impedance spectroscopy. However, due to the frequency range limitations of instruments, we can only see some part of the complete response depending upon the temperature. For modelling the impedance spectrum, an equivalent circuit suitable for the system was designed. In actual incidents, the impedance arc is often depressed, and this leads to the necessity of a constant phase element (CPE). In this case, a constant phase element (CPE) was used instead of a pure capacitor for modelling an equivalent circuit to real impedance data. A constant phase element originates due to the microstructural inhomogeneities inside the sample, and it is equivalent to the distribution of capacitors placed in parallel[126]. The capacitance of the

constant phase element is given by the relation $C = Q^{K}R^{(1-K)/K}$ where the parameter K represents the deviation from ideal capacitive behavior. The value of K is unity for the pure capacitive behavior and zero for the pure resistive behaviour. The values of K are calculated from the slope of log |Z| vs log ν plots in the high-frequency regime[127]. At high frequencies, the corrected modulus is monopolized by the imaginary part of the impedance. The modulus approaches zero, according to $|Z|_{adj} \approx f^{-K}$. Thus the slope on a logarithmic plot has a value of –K at high frequencies. Generally, the K value determines the roughness of the surface. But in the present case, K changes with the temperature, which can be attributed to the formation of ionic charge carriers in comparison to the deformation in the lattice.

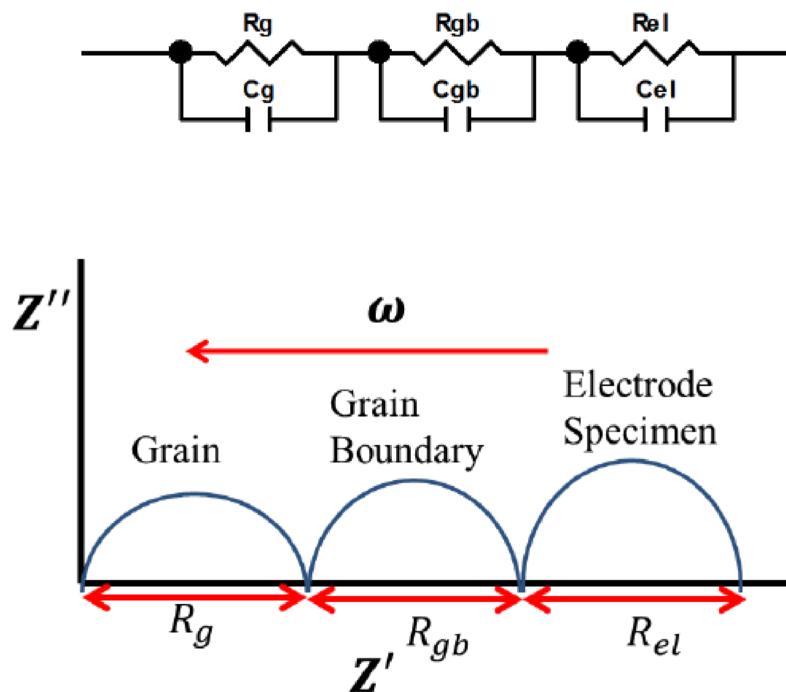

Figure 2.18: The equivalent circuit corresponds to the polycrystalline sample and their frequency response in the complex impedance plot

2.5.2 Conductivity Spectroscopy Technique

Electrical conductivity spectroscopy is the most powerful technique for the exploration of electrochemical properties. The ion dynamics need to be understood in order to tailor the properties of ion-conducting materials. Different research groups and authors have tried various approaches to understand the ion dynamics in a number of systems, such as glasses, nanocomposite, semiconductors, polymers, polycrystals etc., and succeeded in exploring the conduction mechanism[128]. The ion dynamics can be with the help of both conduction and modulus spectra[129]. In the former description, the real part of the conductivity σ' of an ionic conductor can be defined in terms of Jonscher's power law:

$$\sigma_{ac} = \sigma_o + A\nu^n = \sigma_{dc}\left[1 + \left(\frac{\nu}{\nu_h}\right)^n\right] \quad (2.25)$$

where, σ_o is the frequency-independent conductivity, A is constant, ν is the frequency of the applied electric field and ν_h is the crossover frequency from dc to the dispersive conductivity region, n is the power-law exponent, and it represents the degree of interaction between the mobile ions with the lattice with value generally smaller than unity[130][131].

The above equation consists of two parts: (i) frequency-independent part, known as dc conductivity, σ_{dc} and (ii) frequency-dependent ac component. Almond and West proposed crossover frequency as the hopping frequency in their work. The hopping frequency, ν_h and the dc conductivity is associated with each other through the Nernst-Einstein relation:

$$\sigma_{dc} = en_c\mu = \frac{n_c e^2 \gamma \lambda^2}{kT} \upsilon_H \quad (2.26)$$

where n_c is the mobile charge carriers concentration, μ is mobility, e is the electronic charge, k is Boltzmann's constant, T is temperature, λ is hopping distance, and γ is the geometrical factor for ion hopping. The above equation can be used to evaluate the charge carrier concentration

and its variation with temperature. It is already proved that the conducting spectra of ion-conducting materials at different temperatures follow the scaling law known as the time-temperature superstition principle (TTSP), which means that the conductivity isotherm can be superimposed to a single curve using appropriate scaling parameters. This principle can be mathematically expressed as[123]:

$$\frac{\sigma^{'}(\omega)}{\sigma_{dc}} = F(\frac{\upsilon}{\upsilon_s}) \qquad (2.27)$$

where F is a temperature-independent function and is a temperature-dependent scaling parameter. Various types of scaling models have been proposed by different workers, such as Summerfield scaling[132], Roling et al. scaling[133], Sidebottom scaling[134], Baranovskii, and Cordes scaling [135], and Ghosh scaling[123]. All models differ according to the selection of scaling parameters, i.e., hopping frequency. In Summerfield scaling $\sigma_{dc}T$, in Roling et al., scaling ${}^{\sigma_{dc}T}/_{x}$ and in Ghosh scaling ω_H are chosen as the scaling parameter. Among the above scaling, Ghosh scaling is widely applicable because of the automatic consideration of changes in permittivity and the Haven ratio[123].

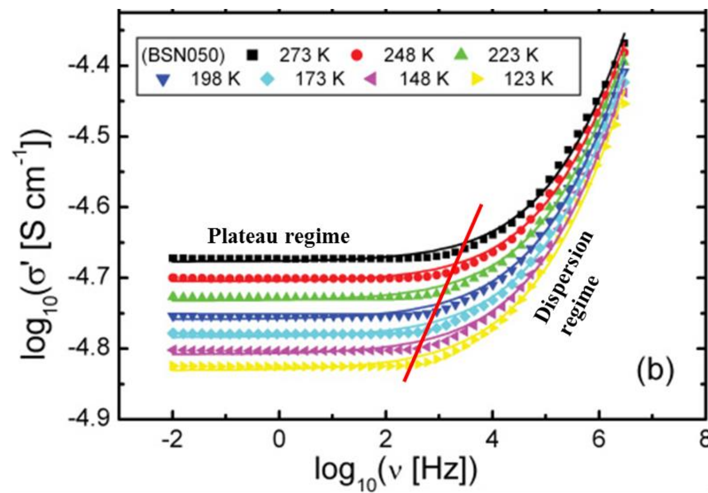

Fig. 2.19: A typical conductivity spectra of a polycrystalline material

2.6 Analysis Techniques

2.6.1 Rietveld Refinement Technique

To understand the properties of investigated compositions in the present work more precisely, their structural information is an essential tool. Among various analysis tools, X-ray diffraction is the most effective and more frequently implemented method. R. M. Rietveld has introduced a structure profile refinement technique for powder diffraction data of Neutron radiation and X-ray. Rietveld's refinement method constructs an effective separation of these overlapping data and allows an accurate evaluation of the structure. Various parameters of these reflections, such as height, width, and position, can be utilized to define several aspects of the structure of materials. In this process, to get the best fit of the theoretical and measured profile, least-square refinement has been carried out. The obtained experimental XR pattern is undergone through the identification of crystalline phases(s) matched with the available materials in the COD database. After the phase identification, individual detailed structure file so-called crystallographic information file (CIF) is taken for further process. A theoretical pattern is simulated by Rietveld refinement software using the CIF file. In order to study the structural and microstructural characterizations following information must be provided (i) instrumental correction factors like peak shift, peak broadening and asymmetry in peak (ii) approximate value of crystallite size and lattice strain. The experimental XRD pattern is refined by simulated XRD pattern through iterative method keeping another parameter as constant to obtain the structural and microstructural parameters. The Marquardt least square fitting method has been used in the present case. The “best fit” between intensities of simulated and experimental XRD pattern is achieved by successive refinement of structural and

microstructural parameters until the parameters are converged. The quantity S_y is minimized through least square method defined as-

$$S_y = \sum_i W_i (I_{oi} - I_{ci})^2 \tag{2.28}$$

Here, $W_i = 1/I_{oi}$, I_{oi} = observed intensity at the ith step and I_{ci} *is* calculated intensity at ith step. The best fit is achieved when S_y attains a minimum value. The value of I_{ci} is obtained by summation of all calculated intensities and background contribution given by;

$$I_{ci} = S\sum_K L_K |F_K|^2 Ø(2\theta_i - \theta_k) P_K A + I_{bi} \tag{2.29}$$

Here, S is the scale factor, L_K contains Lorentz polarization factor and multiplicative factor, k represents Bragg reflection miller indices *hkl*, F_K is the structure for kth Bragg reflection, Ø is a reflection profile function that approximates the effect of aberration due to absorption, specimen displacement, crystallite size, microstrain etc., P_K is the preferred orientation function, A is an absorption factor, I_{bi} is the background intensity of step, $2\theta_K$ is the diffraction angle of kth Bragg reflection.

The Rietveld refinement of the X-ray diffraction pattern is critical process because it requires many calculations due to the involvement of many parameters. For that purpose, sophisticated software is required which correlate the calculated and experimental XRD pattern at each step and so that software should be user-friendly. There are some software available free of cost and are being used by many users worldwide, FullProf software package has been used in the present thesis work for Rietveld refinement purposes. This software package is also used as a profile matching tool without knowledge of the crystal structure. This software is capable of evaluating the various structural and microstructural parameters with the incorporation of all recent development. A typical interface of FullProf software is shown in

Figure 2.20. This software is used to analyze X-ray diffraction of different samples from bulk to nano dimensions[136][137].

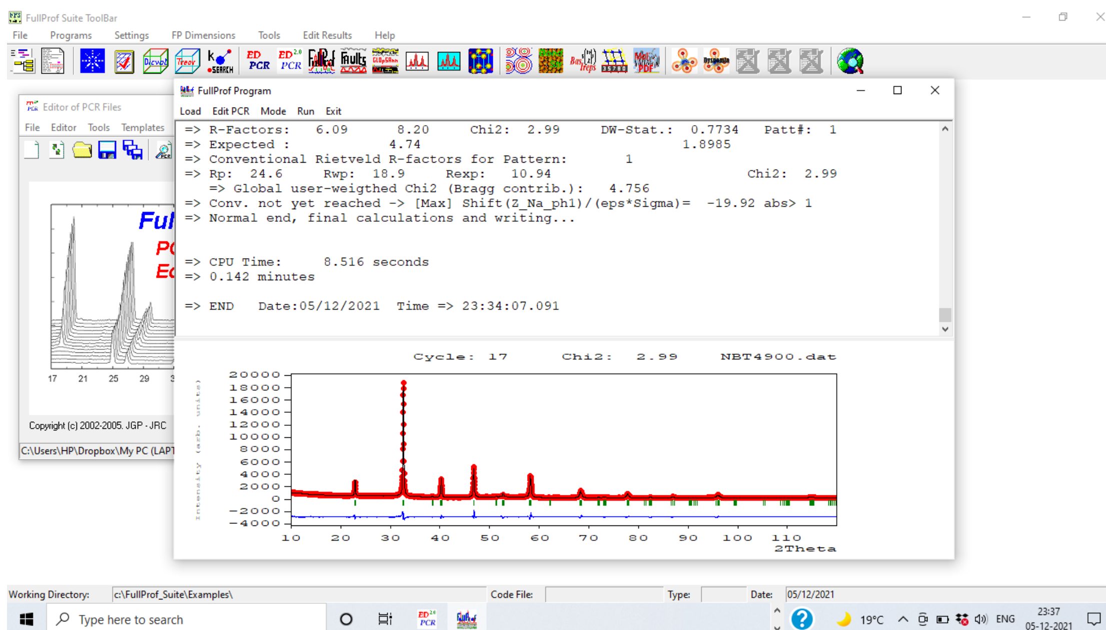

Figure 2.20 A typical FullProf software interface during the Rietveld refinement process

The main features and advantages of FullProf software are

1. The X-ray diffraction data, collected by Laboratory set-up and synchrotron sources, and neutron diffraction sources can be used for refinement through this software.

2. The backgrounds are defined by a variety of functions like constant function, higher-order polynomial through Fourier filtering.

3. The peak shape is modelled in variety of functions for each phase: Lorentzian, Gaussian, pseudo-Voigt, modified Lorentzian, Pearson-VII, split pseudo-Voigt, Thompson-Cox Hashing (TCH) pseudo-Voigt, numerical, the convolution of a double exponential with a TCH pseudo-Voigt.

4. The Rietveld refinement can be performed for multiple phases (upto 16 phases).

5. Two types of functions are available for the modelling of preferred orientation of peak. 6. Absorption corrections for different geometries and micro-absorption correction for the Bragg-Brentano set-up are available.

7. It provides the choice of automatic generation of *hkl* and/or symmetry operators.

8. Magnetic structure refinement can also be performed.

9. Automatic generation of reflections for an incommensurate structure upto 24 propagation vectors.

10. Dependence of the position shifts of Bragg reflections for special kinds of defects.

11. Quantitative analysis has been performed without the need for structure factor calculations.

12. The instrumental resolution function (Voigt function) can be stored in a file, and then the microstructural analysis can be done.

13. Popa-Balzer model can add anisotropic crystallite size and strain.

14. For a better view of the simulated pattern along with the experimental pattern, the square root of intensity is plotted against 2θ.

The quantitative measure of different phases present in a multiphase compound directly depends on the scale factor of Rietveld refinement[138]. For a multiphase system with known molecular weight, the weight fraction phase can be calculated using the relation;

$$W_i = \frac{S_i(ZMV)_i}{\sum_j S_j(ZMV)_j} \tag{2.30}$$

Here, S_i is the scale factor, Z_i is the number of molecules per unit cell, $M_i$is the molecular weight and V_i is the unit cell volume of ith phase present. The density of phase can be evaluated using the following relation-

$$\rho_i = \frac{Z_i M_i}{N_A V_i} \tag{2.31}$$

N_A is Avagadro number. It is important to calculate the relative phase abundances in a multiphase compound for its different scientific and industrial applications. Rietveld analysis was found to be a very successful method to determine the phase fraction of multiphase material.

X-ray diffraction profile fitting by the Rietveld refinement method utilizes an iterative method to minimise different structural and microstructural parameters[138]. These methods refine and adjust different parameters until the residue between experimental intensities (I_{oi}) and calculated intensities (I_{ci}) is minimized. Following residue parameters are used to define the quality of fitting. The residue of structure factor

$$R_F = \frac{\sum_i |\sqrt{I_{oi}} - \sqrt{I_{ci}}|}{\sum_i |\sqrt{I_{oi}}|} \tag{2.32}$$

The residue of Bragg factor

$$R_B = \frac{\sum_i |I_{oi} - I_{ci}|}{\sum_i |I_{oi}|} \tag{2.33}$$

The residue of weighted pattern

$$R_{wp} = \left| \frac{\sum_i W_i (I_{oi} - I_{ci})^2}{\sum_i W_i (I_{oi})^2} \right|^{1/2} \tag{2.34}$$

The residue of expected pattern

$$R_{exp} = \left| \frac{N - P}{\sum_i W_i (I_{oi})^2} \right| \tag{2.35}$$

In all the equation I_i is the intensity of ith Bragg reflection at the end of the refinement, the letter and *I* in suffix represents the observed and calculated intensities. W_i and *N* represents the weight and number of experimental observations, and *P* represents the number of refinable parameters. The refinement process has been continued till convergence of this parameter is reached. The quality of fit is also monitored by “Goodness of fit” (GoF), defined as

$$GoF = \frac{R_{wp}}{R_{exp}} \tag{2.36}$$

For best fit, the *GoF* is approx. 1.00, which means the calculated pattern fully matched with the experimental pattern.

2.6.2 Process of Analyzing the Obtained Data

OriginPro 8.5 program, Soft BV, and the Image-J software were used to examine the structural, optical, and electrical aspects of the tested samples.

2.7 Theoretical Studies

The oxide ion migration pathways were analyzed using the bond valance site energy (BVSE) approach. The bond valance energy landscape for a test oxide ion was calculated using soft-BV software. The details are given below.

2.7.1 Bond Valance Energy-Based Approach

The Bond Valence model is an imperative approach to assess the chemical credibility of inorganic crystal structures. This model is based on the bond-valence sum *(BVS)* rule from Pauling's electrostatic valence concept, which expresses that the sum of all bond valences linked to an atom almost equals the absolute value of its oxidation state. According to this approach, the sum of bond valences, S_{ij}, about any ion, i, is equal to its valence, V_i (i.e. the formal oxidation state

$$V_i = \sum_j S_{ij} \tag{2.37}$$

where the sum runs over all adjacent atoms j of the atom i. The bond valence S_{ij} can be considered as a measure of the electrostatic flux between a cation and an anion. It is directly

related to the strength of the bond and is correlated inversely with bond length. It can be estimated by the following relation:

$$S_{ij} = exp\left(\frac{R_o - R_{ij}}{B}\right) \quad (2.38)$$

where R_o and B are constant parameters and R_{ij} is the interatomic distance between atoms i and j. For many bonds, B is approximated to 0.37. The Bond valence approach is also used to explain the structural distortions from the ideal three-dimensional crystal structure by calculating the global instability index parameter[139][140]. Although the energy barriers obtained by BVS analysis are only relative and not as accurate as the ones obtained by more sophisticated computational methods[141]. The room temperature X-ray Rietveld refined crystallographic information file parameters were used for the bond valance energy calculations, and the BVE landscape and crystal structure were drawn using Vesta software[142]. The spatial resolution in the calculation was set to 0.1 Å. The energy barriers for oxide ion migration were estimated using the BVE landscape.